Journal of Catalysis **182,** 449–455 (1999)
Article ID jcat.1998.2343, available online at http://www.idealibrary.com on IDEAL®

Characterization of Pumice-Supported Ag–Pd and Cu–Pd Bimetallic Catalysts by X-Ray Photoelectron Spectroscopy and X-Ray Diffraction

A. M. Venezia,*,[1] L. F. Liotta,* G. Deganello,*,† Z. Schay,‡ and L. Guczi‡

*ICTPN-CNR, via Ugo La Malfa 153, I-90146 Palermo, Italy; †Dipartimento di Chimica Inorganica, Università di Palermo, Viale delle Scienze, I-90128 Palermo, Italy; and ‡Department of Surface Chemistry and Catalysis, Institute of Isotope and Surface Chemistry, CRC, HAS, P.O. Box 77, H-1525 Budapest, Hungary

Received July 30, 1998; revised October 20, 1998; accepted November 4, 1998

Bimetallic Ag–Pd and Cu–Pd catalysts supported on pumice have been prepared in order to be used in the selective hydrogenation of dienes. The catalysts were obtained by the classical impregnation method and in the case of the Cu–Pd system also by organometallic precursors. They were analysed by X-ray photoelectron spectroscopy (XPS) and X-ray diffraction (XRD). XPS allowed us to determine the surface distribution and chemical state of the two elements; XRD yielded the lattice parameters and allowed us to establish the possible formation of alloys. The two bimetallic systems behave differently. In the case of the Ag-Pd catalysts, Pd particles covered by silver atoms along with highly dispersed monometallic Ag particles interacting with the support were formed, without evidence of alloy formation. The possibility of a layer of silver segregated over the palladium particles would explain the Ag 3*d* binding energy shifts and also the differences between the overall and the surface Ag/Pd atomic ratios. Evidence of alloy formation was found for the Cu–Pd system obtained by impregnation. Analogously, alloy formation was detected in the organometallic samples reduced at higher temperature. An investigation of the oxidation behaviour of the Cu–Pd catalysts revealed a superior oxidation resistance of the alloyed particles. The differences between the Ag–Pd and Cu–Pd systems are discussed in terms of interaction with the support.

Key Words: **pumice-supported Pd–Cu; Pd–Ag bimetallic catalysts; XPS characterization.**

1. INTRODUCTION

Among Group VIII metals palladium is the most active and selective metal for the hydrogenation of acetylenics and diolefins to the corresponding olefins. However, its use has several disadvantages: the activity strongly decreases with the feeds containing sulfur components, the selectivity is restricted by competitive reactions such as the complete saturation of the hydrocarbon and the olefin double bond shift, and oligomerization occurs (1). Synthesis of the bimetallic catalysts consisting of palladium and a second metal deposited on a conventional support eliminates some of the problems listed above (2–4). Addition of a second metal can modify both the hydrogen availability and the strength of diene or alkyne complexation, improving the selectivity to alkene and also extending the lifetime of the catalyst (5). Group VIII metals have an acidic character which depends on their location in the periodic table (6). Such character affects the bonding between the organic substrate and the metal, resulting in a strong complexation and an inhibition of the catalyst activity.

A way of controlling the stability of the intermediates consists in adding an element donating electrons to the metal. Such elements can be found among the Group Ib metals (7). The intimate contact between the two metals is crucial and is governed by the preparation procedure and also by the nature of the support. Moreover, the knowledge of surface composition and structure of bimetallic particles is of primary importance for the adsorption and catalytic phenomena. Quite often the surface composition is indeed very different from the bulk and, as a general rule, the metal with the lower energy of sublimation has a tendency to segregate at the surface (7). Bimetallic-supported catalysts, however, tend to be rather nonideal. Formation of small bimetallic particles on a support is, in many cases, kinetically rather than thermodynamically controlled (8). There is a possibility that the catalyst preparation might not lead to full thermodynamic equilibration. Furthermore, the nature of the precursor compounds and their chemical interaction with the chosen support material can exert a strong influence on the sequence of metal nucleation and reduction. Therefore, the chemical and physical properties of the bimetallic surfaces are not simply related to bulk composition, but to the preferential segregation of one component from the bulk to the surface of the material.

Finally, depending on the relative values of surface tensions at the respective metal–support interfaces, different degrees of interaction between the two metals and the

[1] To whom correspondence should be addressed.

0021-9517/99 $30.00

support could be envisioned. This, in turn, would affect the resulting shape, structure, and composition of the bimetallic particles and in extreme cases precludes the formation of bimetallic particles altogether (8).

In this work, the effects of the second metal, such as silver and copper, on the structure and surface of pumice-supported palladium catalysts are described. The choice of pumice as carrier is dictated by previous studies (9–11) showing an electron donor effect from such support to the metal. This property could favour an appropriate interaction between the two metals. The importance of alloying and of metal–support interaction on the electronic properties of the active metal is stressed.

Two techniques of analysis, X-ray diffraction (XRD) and X-ray photoelectron spectroscopy (XPS), were used. The first technique offers information about the particle sizes and lattice parameters, while the second one provides data on the metal core level binding energy and elemental composition of the surface.

2. EXPERIMENTAL

2.1. Catalyst Preparation

The Ag–Pd and one series of Cu–Pd pumice catalysts were prepared by consecutive impregnation of the acid-treated pumice support (5 m^2/g) (13) with aqueous solution of the precursor nitrates, starting with the palladium solution. Each impregnation was followed by removal of solvent under vacuum and drying in the oven at 353 K. Finally the catalysts were calcined under a stream of oxygen at 773 K for 6 h and then reduced at 623 K for 6 h.

Another set of Cu–Pd pumice catalysts with low copper content was obtained using organometallic precursor. With this procedure aimed at reaching a better copper dispersion (12), the monometallic palladium catalysts were prepared from pentane solution of $Pd(C_3H_5)_2$ according to a previous procedure (13) and subsequently reduced in a stream of H_2 between 258 and 298 K; then the Pd containing samples were contacted with the green-brown solution of (E)-2-ethyl-1-hexenyl-copper (I) (14) of known concentration in $(C_2H_5)_2O$, under nitrogen, at a temperature of 258 K and while stirring it for 3 h. The anchoring reaction

$$\begin{aligned}&(\text{Pd})\text{Pum–OH} + C_4H_9C{=}CHCu(I)\\ &\qquad\qquad\qquad\qquad\quad|\\ &\qquad\qquad\qquad\qquad C_2H_5\\ &\rightarrow (\text{Pd})\text{Pum–OCu} + C_4H_9C{=}CH_2\\ &\qquad\qquad\qquad\qquad\qquad\quad|\\ &\qquad\qquad\qquad\qquad\qquad C_2H_5\end{aligned} \qquad [1]$$

occurred, where Pum represents the pumice and OH indicates the free hydroxyl groups of the support.

The subsequent reduction was carried out at 258 K for 10 min, then at 263 K for 1 h and at 273 K for 30 min. High-purity H_2 (provided by SOL S.p.A. of Palermo) passed through a BTS catalyst (Fluka) for removal of oxygen traces was used for all the reduction treatment. The samples were slowly heated to room temperature and kept 30 min under flowing hydrogen. The chemical composition of the catalysts was determined by atomic absorption spectroscopy (AAS). Henceforth, the figures preceding the metal in the notation of the catalysts indicate the corresponding weight percentage.

2.2. Structural Analysis

XRD measurements, performed with a Philips X-ray diffractometer using nickel-filtered Cu$K\alpha$ radiation, allowed us to obtain the crystallite sizes as well as the lattice parameters of the metal phase. A proportional counter and a 0.05° step size in 2θ were used. The reproducibility on the lattice parameters was estimated to be ±0.005 Å. The metal particle sizes of the reduced catalysts were estimated as volume-averaged crystallite dimension, through the line broadening (LB) of the available reflection peaks using the Scherrer equation according to the method reported in the literature (15).

XPS measurements were performed with a Kratos ES 300 ESCA instrument working in fixed analyser trasmission (FAT) mode using a pass energy of 40 eV. Spectra were generated by Al$K\alpha$ X rays ($h\nu = 1486.6$ eV, 150 W). With a constant line width of the peaks during sample analysis, differential charging was considered absent. The uniform sample charging was eliminated by referencing all the binding energies to the Si 2*p* core level energy from the support, previously found at 103.5 eV (16). Referencing with respect to the C 1*s* peak of the contamination carbon yielded the same energy values. The experimental spectra were resolved into Lorentzian–Gaussian components after background subtraction, using a nonlinear least-square fitting routine. Binding energies and intensity ratios were obtained according to previously described procedures (9, 10). During the analysis, the pressure was in the 10^{-9} Torr (1 Torr = 133.3 Nm^{-2}) range. The powder samples were pressed into a copper grid and then mounted onto the tip of the sample holder rod. The absence of any signal from the copper grid was checked. Further sample treatments were carried out in an atmospheric chamber attached directly to the ESCA machine, thereby preventing air exposure prior to the XPS measurements. The samples underwent hydrogen treatment at 298 or 623 K, depending on the adopted reduction temperature, for 1 h prior to XPS analysis. Then they were pumped while still at a high temperature to eliminate the Pd hydride formation. The organometallic series of Cu–Pd catalysts underwent additional hydrogen and oxygen treatments.

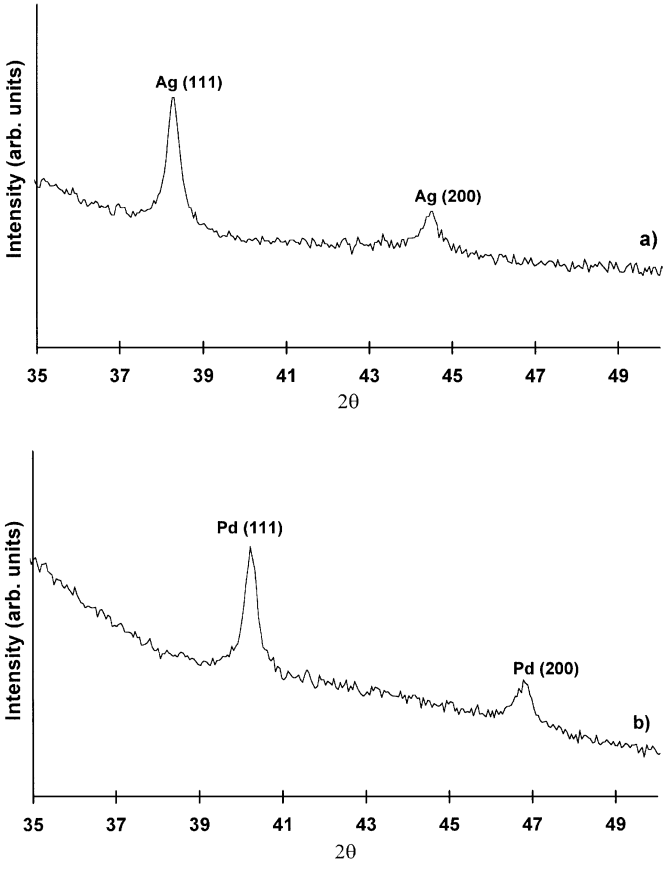

FIG. 1. X-ray diffractograms of (a) 0.5Ag/pumice and (b) 0.05Ag–0.25Pd/pumice catalysts.

3. RESULTS AND DISCUSSION

3.1. Ag–Pd Catalysts

In Figures 1a and 1b the X-ray diffractograms relative to the monometallic 0.5Ag/pumice and to the bimetallic 0.05Ag–0.25Pd/pumice, respectively, are reported. Using the appropriate (111) and (200) reflections, the metal particle sizes and the lattice parameters of the metallic particles were obtained. As shown in Fig. 1b, the diffraction pattern of the bimetallic catalyst does not contain any of the silver reflections, unlike in the case of the monometallic 0.05Ag/pumice, for which a diffraction pattern similar to that shown in Fig. 1a but of smaller intensity was observed. Therefore, the silver loading of the bimetallic catalysts was above the detection limit of the X-ray diffraction technique, and the lack of silver-related reflections in the Ag–Pd catalyst diffractogram of Fig. 1b should be attributed to highly dispersed silver atoms rather than to the low concentration. In Table 1 the surface atomic ratios arising from chemical analysis (CA) and XPS analysis are reported along with the lattice parameters and the particle diameters. Among the bimetallic catalysts, a decrease of the Pd particle size with the increasing Ag/Pd atomic ratio is observed in Table 1. The invariance of the Pd-related lattice parameters upon addition of silver would indicate that the bulk of the palladium particles is monometallic. The Ag/Pd atomic ratios derived from XPS intensity data are larger than the corresponding overall values. The discrepancy may be explained by two different situations: (a) higher dispersion of monometallic silver particles as compared to the monometallic palladium particles, in agreement with the XRD results; (b) segregation of silver on the Pd aggregates. Obviously both cases may coexist and, moreover, formation of small ($\leq$15 Å) alloyed particles, not detectable by the X-ray diffraction technique, cannot be ruled out. The surface enrichment of silver in various Ag–Pd systems has been already observed and attributed to the lower surface energy of silver with respect to palladium (17, 18).

TABLE 1

Pumice-Supported Catalyst Ag/Pd Atomic Ratios from Chemical Analysis (CA) and from XPS Analysis

Catalyst	Ag/Pd_{CA} (at% Ag)	Ag/Pd_{XPS} (at% Ag)	d_{Pd} (Å)	d_{Ag} (Å)	a_{Pd} (Å)	a_{Ag} (Å)
0.28Pd			139		3.888	
0.05Ag–0.25Pd	0.19(16)	1.7(56)	210		3.894	—
0.08Ag–0.25Pd	0.28(22)	1.0(50)	187		3.895	—
0.06Ag–0.17Pd	0.36(27)	1.5(60)	119		3.895	—
0.05Ag				400		4.091
0.50Ag				300		4.082

Note. Pd and Ag particle sizes, d, and lattice parameters, a, are determined by XRD. In parentheses are indicated the corresponding atomic percentages of the silver. Bulk values: $a_{Pd} = 3.890$ Å; $a_{Ag} = 4.086$ Å.

In Fig. 2, as an example of typical Pd 3*d* and Ag 3*d* photoelectron spectra of the catalysts, the experimental peaks of the sample 0.05Ag–0.25Pd/pumice along with the fitted curves are shown. The metallic state is indicated by the asymmetric line shapes exhibited by both elements and fitted using exponential tails on the high binding energy sides (19). The binding energies of the main spin orbit component $3d_{5/2}$ of the doublets are presented in Table 2. Two

TABLE 2

Pd $3d_{5/2}$ and Ag $3d_{5/2}$ of the Pumice-Supported Bimetallic and Monometallic Catalysts (the Full Width at Half Maximum Is Given in Parentheses)

Catalyst	Pd $3d_{5/2}$ (eV)	Ag $3d_{5/2}$ (eV)	ΔE_{Ag} (eV)	ΔE_{Pd} (eV)
0.28Pd	335.1 (2.2)			−0.4
0.05Ag–0.25Pd	334.9 (2.1)	367.1 (1.8)	−1.2	−0.5
0.08Ag–0.25Pd	334.9 (2.1)	367.0 (2.0)	−1.3	−0.5
0.06Ag–0.17Pd	334.9 (2.2)	367.0 (1.9)	−1.3	−0.5
0.05Ag	—	367.9 (2.4)	−0.4	—

Note. The corresponding chemical shifts with respect to the bulk energies, ΔE_{Ag} and ΔE_{Pd}, are given. $Pd_{bulk}3d_{5/2} = 335.5$ eV (9); $Ag_{bulk}3d_{5/2} = 368.3$ eV (21).

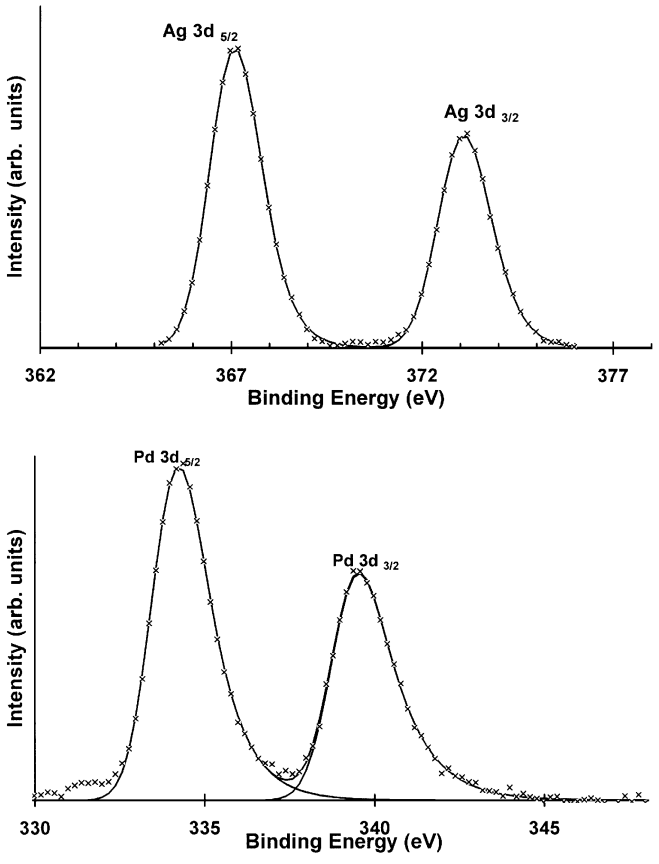

FIG. 2. Pd 3*d* and Ag 3*d* photoelectron spectra of the 0.05Ag–0.25Pd/pumice catalysts.

points should be considered: (a) the Ag $3d_{5/2}$ binding energies of the bimetallic catalysts are lower than the corresponding energies of the monometallic ones; (b) the Pd- and Ag-related binding energies of the monometallic pumice catalysts are both lower than the reference pure metal bulk values. The binding energy of the Ag $3d_{5/2}$ of the Ag–Pd catalysts shifts by about −0.90 eV relative to the monometallic Ag/pumice and by about −1.2 eV with respect to the silver bulk; this is different from the Pd $3d_{5/2}$, which maintains the same value with respect to the monometallic, but is −0.6 eV below the corresponding energy for the palladium bulk.

A previous XPS study on coevaporated Pd_xAg_{1-x} alloys showed negative shifts for silver and positive shifts for palladium with respect to the pure metals (20). In a subsequent investigation of carbon-supported bimetallic palladium–silver clusters (21), positive cluster size shifts were obtained by correcting the experimental Ag 3*d* binding energy changes for the alloy shifts (20). Therefore, the negative ΔE values listed in Table 2 cannot arise from size effects (21). As established earlier, pumice is not a completely inert carrier, inasmuch as it affects the electron density of the supported metal (9, 10, 22). Previous XPS analysis of pumice-supported palladium catalysts had shown negative Pd 3*d* binding energy shift as compared to the unsupported metal. The shift was attributed to the electron donor property of the support determined by its alkali ion content (10). According to these previous results, an Ag 3*d* binding energy shift of −0.4 eV is also found between the monometallic Ag catalyst and the pure Ag metal. Moreover, while the Pd 3*d* shifts of the Ag–Pd samples are typical of the monometallic palladium on pumice (22), the corresponding Ag 3*d* shifts, ΔE_{Ag}, relative to the monometallic Ag on pumice, listed in Table 2, are considerably larger. Considering that, according to a previous XPS study on Ag–Pd alloys (20), the shifts on the Ag 3*d* binding energy of silver atoms embedded in a palladium matrix can be as high as 1 eV, the present values could be attributed to the interaction with the palladium. Within the accuracy of the data (±0.1 eV) the line widths of the Pd 3*d* and Ag 3*d* peaks are constant among the different catalysts. The smaller Ag 3*d* width of the Ag–Pd samples with respect to the monometallic Ag catalyst could be due to variation of the local *d*-density of states at the Fermi level (23). Such density tends to decrease when the element is surrounded by different elements like being embedded in a support matrix or being alloyed.

Particles formed by a core of palladium covered by a layer of silver atoms would be in accord with the intensity ratios and with the binding energy shifts of the XPS peaks. The silver layer as suggested from the absence of a silver X-ray diffraction pattern cannot be thicker than 15 Å. In addition, the decrease of the particle size with Ag/Pd atomic ratio, observed in Table 1, may be ascribed to an inhibiting effect of the silver atoms on the growth of the Pd particles. On the other hand, on the basis of the experimental results, the possibility of monometallic particles with silver in a highly dispersed phase cannot be ruled out.

3.2. Cu–Pd Catalysts

In Table 3 the Cu–Pd catalysts with the chemical analysis and XPS-derived surface atomic ratios, the diameters, and the lattice parameters are reported. Similarly to the Ag–Pd samples, the surface Cu–Pd atomic ratios are larger than the overall ratios. On average, the series prepared by the organometallic route and therefore involving lower reduction temperature is characterised by smaller Pd particle diameters. The presence of Cu does not have a distinct effect on the particle sizes, contrary to what was observed on Cu–Pd particles supported on carbon and on silica (3, 24), for which a decrease in the first case and an increase in the second case of the Pd crystallite size with increasing Cu content were observed. For most of the catalysts, the diffraction technique does not detect any metallic or oxide copper phase. On the other hand, the palladium-related diffraction peaks allowed the calculation of the lattice parameters of the corresponding phase. In the series of bimetallic catalysts prepared from nitrates, involving higher reduction temperature, a change of the lattice parameter with respect to the

TABLE 3

Pumice-Supported Catalyst Cu/Pd Atomic Ratios As Derived from Chemical Analysis (CA) and XPS Analysis, Pd and Cu Particle Sizes, *d*, and Lattice Parameters, *a*, As Determined by XRD

Catalyst	Cu/Pd_{CA} (at%)	Cu/Pd_{XPS} (at%)	d_{Pd} (Å)	d_{Cu} (Å)	a_{Pd} (Å)	a_{Cu} (Å)
0.28Pd[a]			139		3.888	
0.05Cu–0.24Pd[a]	0.35 (26)	2.0 (67)	250		3.875	
0.06Cu–0.20Pd[a]	0.50 (33)	1.5 (60)	264		3.873	
0.08Cu–0.27Pd[a]	0.50 (33)	1.5 (60)	147		3.859	
0.22Cu–0.28Pd[a]	1.32 (57)	2.9 (74)	127		3.849	3.648
0.50Cu[a]				400		3.611
1.5Pd[b]			110		3.890	
0.6Pd[b]			63		3.883	
0.05Cu–1.5Pd[b]	0.05 (5)	0.2 (17)	78		3.901	
0.05Cu–0.6Pd[b]	0.10 (9)	0.3 (23)	76		3.883	
0.05Cu[b]						

Note. In parentheses the copper percentages are given. Bulk values: $a_{Pd} = 3.890$ Å; $a_{Cu} = 3.615$ Å.

[a] These catalysts have been prepared by impregnation and the X-ray diffraction and XPS-derived values refer to the samples reduced at 623 K.

[b] These catalysts have been prepared by organometallic route and the X-ray diffraction and XPS-derived values refer to the samples reduced at room temperature.

one relative to the monometallic palladium catalyst is observed. Such a change implies the formation of alloy phases. Using previous data of Cu–Pd alloy lattice parameters (25), from the unit cell edge of the Cu–Pd catalysts (Table 3), the corresponding alloy compositions listed in Table 4 are determined. The lower Cu content of the alloys with respect to the overall loading indicates that most of the copper must be present as highly dispersed monometallic species. The differences between the atomic ratios from chemical analysis and from XPS analysis of Table 3 would accordingly be explained. To distinguish the effect of temperature from the effect of the preparation procedure, sequential reduction and oxidation have been carried out, in the pretreatment chamber of the XPS spectrophotometer, on selected samples obtained from the organometallic precursor. Following the treatments, the Pd 3*d* and the Cu 2*p* spectra change. In Table 5 the corresponding binding energies along with

TABLE 4

Alloy Composition of the Bimetallic Particles of the Pumice-Supported Catalysts As Derived from the Lattice Parameters

Catalyst	Alloy composition (at%Cu)
0.05Cu–0.24Pd	6
0.06Cu–0.20Pd	6
0.08Cu–0.27Pd	12
0.22Cu–0.28Pd	16

Note. The catalysts have been prepared by impregnation and reduced at 623 K.

TABLE 5

Binding Energy of Pd $3d_{5/2}$ and Cu $2p_{3/2}$, and Cu/Pd Atomic Ratios after the Different Treatments of the Pumice Catalyst Prepared by the Organometallic Precursor

Catalyst	Treatment	Pd $3d_{5/2}$ (eV)	Cu $2p_{3/2}$ (eV)	Cu/Pd
0.05Cu–1.5Pd	H_2 (298 K)	335.7	931.7, 933.9	0.2
	H_2 (623 K)	334.8	931.9	0.1
	Air (623 K)	336.7	933.8	0.2
	H_2 (623 K)	334.5	932.1	0.1
1.5Pd	H_2 (298 K)	334.8		
	H_2 (623 K)	334.8		
0.5Cu	H_2 (298 K)		932.4, 933.8	
	H_2 (623 K)		932.4	

Note. The binding energies of the corresponding monometallic pumice catalysts after reduction are also reported.

the Cu/Pd atomic ratios as obtained from the XPS intensity data of the 0.05Cu–1.5Pd/pumice catalyst are reported. For comparison, the binding energies of the monometallic pumice catalysts are also given. The Cu $2p_{3/2}$ spectra after the various treatments are shown in Fig. 3. The hydrogen treatment at 298 K reduces palladium completely, whereas it reduces copper only partially, as shown in Fig. 3a. The spectrum contains two components, one due to Cu metal and the other to CuO which is characterised by the presence of a shake-up satellites at around 8 eV above the main photoelectron transition (26). The reducing treatment at 623 K produces metal copper characterised by the Cu $2p_{3/2}$ peak at 931.9 eV, which is about 0.4 eV below the usual binding energy of the metallic copper (26). This shift allows us to discriminate between Cu^+ and Cu^0 states, not discerned by the XPS spectra because of the same Cu 2*p* binding energies (27). The Auger spectra, different for the two states, could not be used here because of the poor resolution. The observed negative shift with respect to the bulk metal copper may be indicative of the metallic state affected either by support interaction or by alloying (3, 9) considering that in the case of the Cu^+ species an electron donation would not change its binding energy. Moreover, as seen in Table 5, the monometallic copper catalyst has a Cu $2p_{3/2}$ value similar to that of the pure bulk copper, and therefore the changes observed in the bimetallic catalysts could be attributed to the alloying effect. It is interesting to notice that the Pd $3d_{5/2}$ binding energy typical of the metallic state obtained after reduction at 298 K shifts towards lower values after reduction at 623 K, yielding the binding energy found for the pumice-supported palladium catalysts (9). The presence of the copper oxide in close proximity of the palladium metal clusters may neutralise, in a sense, the electron donor property of the support, thereby shifting the Pd $3d_{5/2}$ binding energies to the typical Pd bulk values (9, 10). The absence of electronic effect due to copper on the palladium is also in agreement with a previous FTIR CO

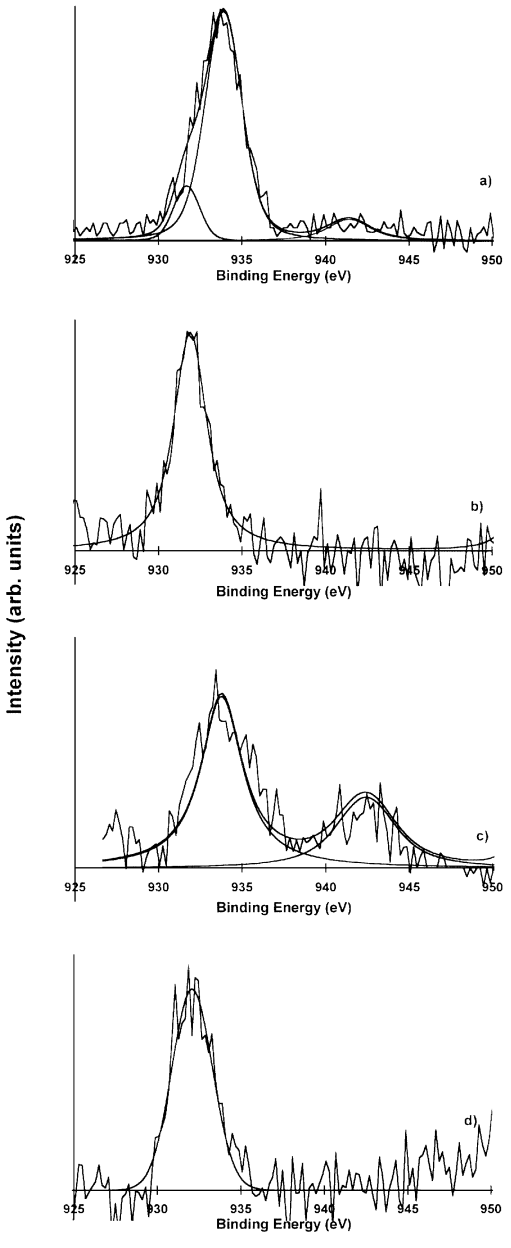

FIG. 3. Cu $2p_{3/2}$ photoelectron peak of the 0.05Cu–1.5Pd/pumice catalyst after the sequential treatment. (a) H_2 at 298 K; (b) H_2 at 623 K; (c) air treatment at 623 K; (d) H_2 at 623 K.

adsorption study (3). After air treatment at 623 K, binding energies typical of PdO and CuO are obtained. The satellite of the corresponding Cu $2p_{3/2}$ transition, in Fig. 3c, is now in the appropriate intensity ratio with the main peak (26).

The variation of the XPS-derived Cu–Pd atomic ratio indicates that copper diffuses inwards upon hydrogen treatment at high temperature whereas it is driven to the surface during the air treatment. Probably the interaction with oxygen represents the driving force for the copper surface segregation. In Table 6 the particle sizes and lattice parameters of the organometallic prepared samples after different treatments are listed along with the at% Cu in the alloy as derived from the lattice parameters. Unlike XPS, which probes the outermost layers of a sample, XRD, as a bulk technique, detects palladium metal still present after the air treatment at 623 K. Sintering of Pd particles at 623 K under the two different gas environments, hydrogen and air, occurs. The lattice parameters observed in 0.05Cu–1.5Pd and 0.05Cu–0.6Pd, upon H_2 treatment at 623 K, are consistent with alloys of 6 and 10 at% in copper, respectively (25), which is closely comparable to the overall composition given in Table 3. The composition of the alloyed particles does not change upon air treatment, as shown by the invariance of the corresponding lattice parameters. Such occurrence indicates that the metal components of these particles are resistant to oxidation, unlike the monometallic species of copper and palladium, which, as shown previously by the XPS spectra, are easily oxidised. It is interesting to note that in the case of the samples prepared by impregnation, containing a larger amount of copper, and treated for longer times at higher temperature, the alloy has a lower copper content relative to the overall composition. On the contrary the samples prepared by the organometallic route and reduced at high temperature for only 1 h contain alloyed particles with the overall catalyst composition. This result indicates that the anchoring of the second metal to an already reduced metal catalyst favours alloying between the two metals during the second reduction step. An analogous conclusion was drawn in a study of Pd–Sn and Pd–Sb bimetallic catalysts supported on alumina where the organometallic precursors yielded supported alloys in contrast with the method of the inorganic precursors in which no interaction between the two metals was found (28).

TABLE 6

Particle Size, *d*, and Lattice Parameters, *a*, Relative to the Metal Phase after Different Treatment of the Pumice-Supported Catalysts

Catalyst	Treatment	d_{Pd} (Å)	*a* (Å)	Alloy composition (at% Cu)
1.5%Pd	H_2 (298 K)	110	3.899	
	H_2 (623 K)	200	3.885	
	Air (623 K)	274	3.887	
	H_2 (623 K)	289	3.887	
0.6%Pd	H_2 (298 K)	63	3.883	
	H_2 (623 K)	200	3.881	
	Air (623 K)	350	3.883	
	H_2 (623 K)	410	3.883	
0.05Cu–1.5Pd	H_2 (298 K)	78	3.901	
	H_2 (623 K)	214	3.873	6
	Air (623 K)	276	3.876	6
	H_2 (623 K)	290	3.873	6
0.05Cu–0.6Pd	H_2 (298 K)	76	3.883	
	H_2 (623 K)	200	3.866	10
	Air (623 K)	266	3.866	10
	H_2 (623 K)	187	3.866	10

4. CONCLUSION

A combination of the surface technique, as XPS, and the bulk technique, as X-ray diffraction, has allowed us to determine the most likely structure of bimetallic catalysts supported on pumice. The Ag–Pd and the Cu–Pd systems seem to behave differently. In the first case both techniques suggest the formation of palladium particles, interacting with pumice, and covered by a layer of silver atoms. The presence of highly dispersed silver particles interacting with the support is also possible and in accord with the binding energy shifts.

The Cu–Pd samples, prepared by two procedures, impregnation and organometallic route, in addition to monometallic copper phase, contain alloys with composition derived from the corresponding lattice parameter. The binding energies of the Pd 3*d* reflect the interaction with the support, and those relative to Cu 2*p* contain contribution from the alloying state. The organometallic procedure, followed by reduction at high temperature, favours the alloy formation. Changes in the atomic ratios Cu/Pd upon H_2 and air treatments at high temperature are attributed to inward diffusion of copper driven by the formation of alloy in one case and outward diffusion of copper driven by the oxide formation in the second case.

The different behaviour exhibited by the Ag–Pd and Cu–Pd catalysts, with silver-decorated palladium particles and dispersed silver particles in one case and mixture of monometallic and alloyed particles in the other case, could be a consequence of the stronger interaction, indicated by the XPS binding energy shifts, of silver with the pumice support.

ACKNOWLEDGMENT

The authors acknowledge CNR (Consiglio Nazionale delle Ricerche) and MTA (Hungarian Academy of Science) for the bilateral program grant and also the "Progetto Finalizzato M.S.T. A.-II."

REFERENCES

1. Boitiaux, J. P., Cosyns, J., Derrien, M., and Leger, G., *Hydrocarbon Process.*, 51 (1985).
2. Iglesia, I., and Boudart, M., *J. Catal.* **81**, 204 (1983).
3. Skoda, F., Astier, M. P., Pajonk, G. M., and Primet, M., *Catal. Lett.* **29**, 159 (1994).
4. Gustafson, B. L., and Wehner, P. S., *Appl. Surf. Sci.* **52**, 261 (1991).
5. Sárkány, A., Zsoldos, Z., Stefler, Gy., Hightower, J. W., and Guczi, L., *J. Catal.* **157**, 179 (1995).
6. Pearson, R. G., *in* "Hard and Soft acids and Bases" (Dowden, Hutchinson, and Ross, Eds.). 1973.
7. de Boer, F. R., Boom, R., Miedema, A. R., *Physica B* **101**, 294 (1980).
8. Schwank, J., *in* "New Trends in CO Activation" (L. Guczi, Ed.). Stud. Surf. Sci. Catal., Vol. 64, p. 225. 1991.
9. Venezia, A. M., Duca, D., Floriano, M. A., Deganello, G., and Rossi, A., *Surf. Interface Anal.* **19**, 543 (1992).
10. Venezia, A. M., Rossi, A., Liotta, L. F., Martorana, A., and Deganello, G., *Appl. Catal. A* **147**, 81 (1996).
11. Venezia, A. M., Parmaliana, A., Mezzapica, A., and Deganello, G., *J. Catal.* **172**, 463 (1997).
12. Travers, C., Bournonville, J. P., and Martino, G., *in* "Proceedings, 8th International Congress on Catalysis, Berlin, 1984," Vol. IV, p. 891. Dechema, Frankfurt-am-Main, 1984.
13. Fagherazzi, G., Benedetti, A., Deganello, G., Duca, D., Martorana, A., and Spoto, G., *J. Catal.* **150**, 117 (1994).
14. Normant, J. F., Cahiez, G., Bourgain, M., Chuit, C., and Villieras, *J. Bull. Soc. Chim. Fr.*, 1656 (1974).
15. Klug, H. P., and Alexander, L. E., "X-ray Diffraction Procedures for Polycrystalline and Amorphous Materials." Wiley, New York, 1954.
16. Venezia, A. M., Floriano, M. A., Deganello, G., and Rossi, A., *Surf. Interface Anal.* **18**, 532 (1992).
17. Ponec, V., and Bond, G. C., "Catalysis by Metals and Alloys." Stud. Surf. Sci. Catal., Vol. 95. 1995.
18. Allison, E. G., and Bond, G. C., *Catal. Rev.* **7**, 233 (1972).
19. Doniach, S., and Sunjic, M., *J. Phys. C* **3**, 285 (1970).
20. Steiner, P., and Hufner, S., *Solid State Commun.* **73**, 79 (1981).
21. Ptacek, P., and Bastl, Z., *Appl. Surf. Sci.* **45**, 319 (1990).
22. Venezia, A. M., Rossi, A., Duca, D., Martorana, A., and Deganello, G., *Appl. Catal. A* **125**, 113 (1995).
23. Wertheim, G. K., and Citrin, P. H., *in* "Topics in Applied Physics" (M. Cardona and Ley, Eds.), Vol. 26, p. 197. Springer-Verlag, Berlin, 1978.
24. Benedetti, A., Fagherazzi, G., Pinna, F., Rampazzo, G., Selva, M., and Strukul, G., *Catal. Lett.* **10**, 215 (1991).
25. Burch, R., and Buss, R. G., *J. Chem. Soc. Faraday Trans. 1* **71**, 913 (1975).
26. Wagner, C., Riggs, W., Davis, L., Moulder, J., and Muilenberg, G., "Handbook of X-ray Photoelectron Spectroscopy," Perkin–Elmer, Physical Electronics Division, Eden Prairie, MN, 1979.
27. Sepulveda, A., Marquez, C., Rodrigues-Ramos, I., Guerrero-Ruiz, A., and Fierro, J. L. G., *Surf. Interface Anal.* **20**, 1067 (1993).
28. Aduriz, H. R., Bodnariuk, P., Coq, B., and Figueras, F., *J. Catal.* **119**, 97 (1989).